Published by IOP Publishing for Sissa Medialab

Received: *October 31, 2025*
Accepted: *November 14, 2025*
Published: *January 9, 2026*

26th International Workshop on Radiation Imaging Detectors
Bratislava, Slovakia
6–10 July 2025

Measurement of dual-component attenuation length in square BCF-92 and round Y11 wavelength-shifting fibers

A.F.B. Isabel,[a] F. Kellerer,[b] P. Saharia,[b] R.C. Sousa,[a] J.M.R. Teixeira,[a] J.M.F. dos Santos,[a] N. Lopez-March,[b] C.A.O. Henriques,[a] J. Martin-Albo[b] and C.M.B. Monteiro[a,*]

[a] *LIBPhys-UC, LA-REAL, Department of Physics, University of Coimbra, Rua Larga, 3004-516 Coimbra, Portugal*
[b] *Instituto de Física Corpuscular (IFIC), CSIC & Universitat de València, Calle Catedrático José Beltrán, 2, Paterna, E-46980, Spain*

E-mail: cristinam@uc.pt

Abstract: Wavelength-Shifting (WLS) fibers convert ultraviolet and blue scintillation light into green wavelengths, enabling efficient light collection in particle physics detectors. By reducing sensitivity to background noise, these fibers improve signal quality and detection accuracy.

A key parameter affecting their performance is the attenuation length, defined as the distance over which the transmitted light intensity decreases by a factor of 1/e.

We report measurements of the dual-component attenuation length of square double-clad BCF-92 fibers (Saint-Gobain) and round Y11 fibers (Kuraray). Light transmission was studied using a pulsed source, and the attenuation profile was fitted with a double-exponential model to extract short- and long-component parameters. Two independent methods, namely using a spectrophotometer and using a PMT readout, were applied, yielding consistent results.

Systematic tests performed under varying fiber and environmental conditions showed no significant variations, demonstrating the robustness and reproducibility of the measurements.

The experimental setups, data-analysis methods, and implications for scintillation-detector design are presented and discussed.

Keywords: Scintillators and scintillating fibres and light guides; Spectral responses; Double-beta decay detectors; Particle tracking detectors (Gaseous detectors)

*Corresponding author.

https://doi.org/10.1088/1748-0221/21/01/C01007

Contents

2026 JINST 21 C01007

1 Introduction

Wavelength-shifting (WLS) fibers convert blue into green light and, when coated with Tetraphenyl Butadiene (TPB), which converts vacuum ultraviolet (VUV) photons to blue, they enable an efficient conversion from VUV to green, allowing for detection with visible-sensitive photosensors [1].

Figure 1 illustrates the basic process: blue light entering the fiber is absorbed by fluorescent dopants in the core and re-emitted at longer wavelengths, typically red-shifted by tens of nanometers, re-emitting approximately 50–80% of the absorbed energy. The re-emitted green light is guided along the fiber by total internal reflection, ensuring efficient transport to remote photodetectors while minimizing losses [2]. The dopant concentrations are optimized to maximize light yield and minimize attenuation, thereby enhancing fiber performance.

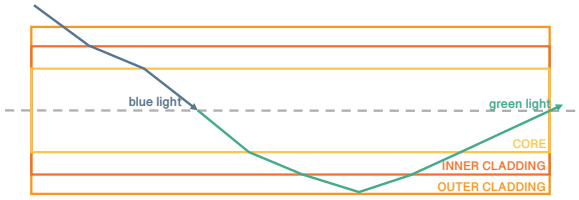

Figure 1. Schematic of the wavelength-shifting process and light guiding inside a double-clad fiber.

By guiding light from the point of interaction to remote photodetectors, WLS fibers minimize signal losses and improve the overall signal-to-noise ratio [3].

A key parameter when using WLS fibers is the attenuation length, which indicates how far light can travel in the fiber before significant attenuation occurs, 1/e.

In this work, the optical performance and attenuation length of Saint-Gobain BCF-92 double-clad square fibers and Kuraray Y11 double-clad round fibers are studied. These studies aim contributing to incorporating WLS fibers in NEXT-HD, the next phase of the Neutrino Experiment with a Xenon Time Projection Chamber (NEXT) [4].

1.1 Wavelength-sifting fibers

WLS fibers are produced in several configurations and optical characteristics. For assessing the present studies, a green-enhanced bialkali PMT, with a quantum efficiency of approximately 26% at 450 nm, was used, well suited for detecting the emitted light [5, 6]. Both Kuraray Y11 and BCF-92 have a polystyrene core and emit in a similar wavelength range [7]. Table 1 summarizes the main properties of both fibers.

Table 1. Main characteristics of the BCF-92 and the Y11 fibers.

	BCF-92	**Y11**
Emission peak / color	492 nm / green	476 nm / green
Absorption peak / color	405 nm / blue	430 nm / blue
Refractive index	1.59 (core); 1.49 (PMMA cladding); 1.42 (fluor-acrylic cladding)	
Density [g/cc]	1.05 (core); 1.19 (PMMA cladding); 1.43 (fluor-acrylic cladding)	

Figure 2 shows both absorption and emission spectra of BCF-92 (left) and Y11 (center).

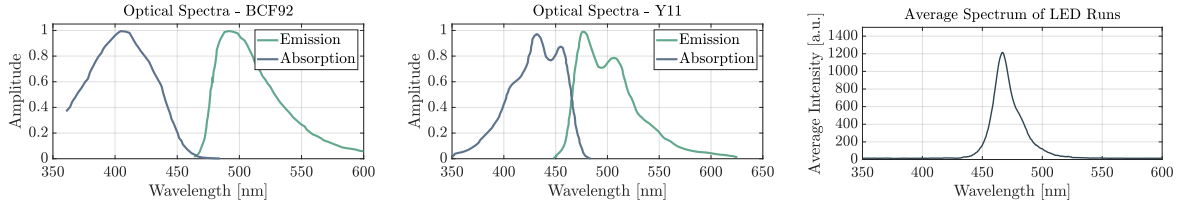

Figure 2. Absorption and emission spectra for the BCF-92 (left) and the Y11 (center) fibers and average LED emission spectrum (right).

While the Stokes shift provides an indication of the separation between emission and absorption peaks, the extent of self-absorption losses ultimately depends on the spectral overlap between both bands, which is influenced by both the shift magnitude and the bandwidth of each spectrum.

BCF-92 exhibits a much clearer separation between absorption and emission bands, whereas Y11 presents a larger spectral overlap, with implications for self-absorption losses. In BCF-92, the emission occurs at wavelengths where absorption is already negligible, minimizing re-absorption of emitted photons and favoring efficient light transport along the fiber. The partial overlap in Y11 increases the probability of emitted photons to be re-absorbed within the fiber core, leading to reduced light yield and poorer transmission efficiency, particularly over longer fiber lengths.

1.2 Experimental setup

Data were acquired from two different setups: one with the light being collected with a Thorlabs CCT10 spectrometer [8], and the other with a PMT [9]. Both setups were assembled inside a light-tight box reducing noise from ambient light.

2026 JINST 21 C01007

1.2.1 Spectrophotometer setup

In the spectrophotometer setup, the fiber was housed inside the enclosure together with a pulsed blue LED, a collimator, an optical fiber linked to the CCT10 spectrometer, and supporting structures for alignment. Prior to measuring the fiber response, the LED emission spectrum was characterized by positioning the spectrophotometer fiber directly in front of the LED, as depicted in figure 3 (left).

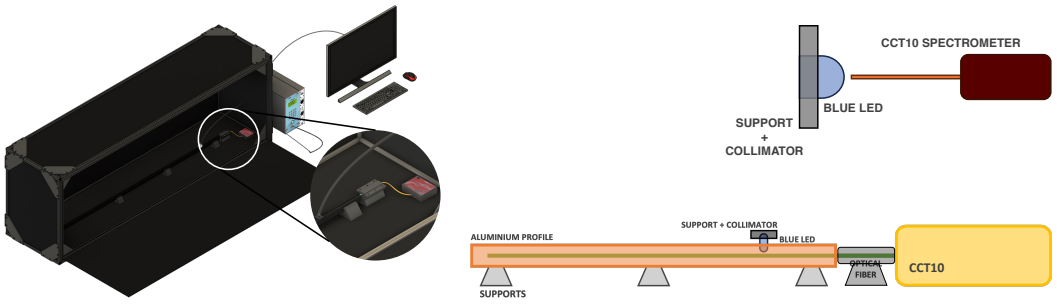

Figure 3. Schematics of the spectrophotometer setup for attenuation length measurements (left), for LED emission spectrum acquisition (top right) andthe CCT10 setup (bottom right).

The peak emission of the BCF-92 occurs at 467 nm, making the LED emission suitable for the WLS fibers (figure 2 (right)).

1.2.2 PMT setup

The PMT setup shares the same light-tight box and support structures, with the CCT10 spectrophotometer replaced by a PMT. The setup includes the fiber mounted on aluminum profiles, the same pulsed blue LED with collimator, and the PMT positioned at the fiber end, as depicted in figure 4 (left).

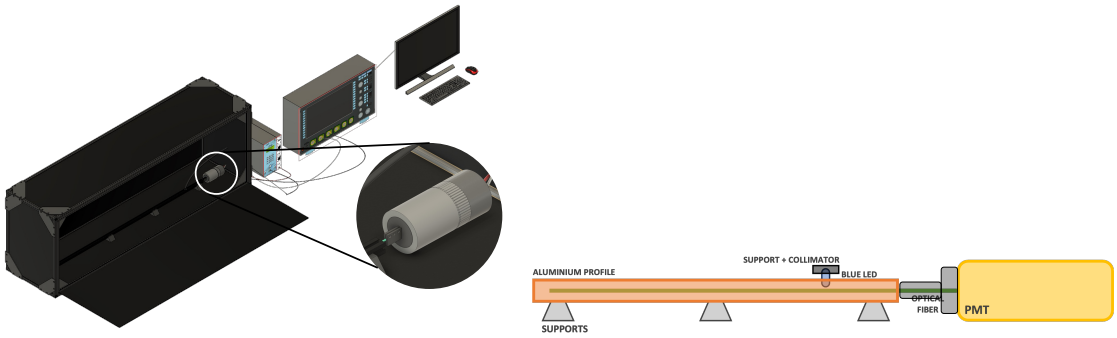

Figure 4. Schematics of the PMT setup with zoom (left) and detail of the PMT setup (right).

Measurements were performed by placing the LED at different positions along the fiber and the waveforms were collected via a LeCroy waverunner on a local computer for offline analysis.

2026 JINST 21 C01007

2 Methodology

The system was first verified for light leaks, after which the photomultiplier tube (PMT) was calibrated in terms of single-photon with LED illumination. This calibration provided the reference gain necessary for quantifying the number of detected photons and evaluating the performance of the fibers in subsequent measurements.

Spectral measurements were performed using a CCT10 spectrophotometer for wavelength-resolved information on the light propagated to the fiber end. The fiber was illuminated with the same LED and emission spectra were acquired for the different distances between the LED source and the fiber input of the CCT10. The acquired spectra were integrated over the full wavelength range and the total light output was plotted as a function of distance. The resulting attenuation curve was fitted with a two-exponential model to extract both short and long attenuation components, providing complementary information to the PMT-based analysis:

$$I(x) = I_{\text{os}} \cdot \exp\left(-\frac{x}{L_{\text{os}}}\right) + I_{\text{ol}} \cdot \exp\left(-\frac{x}{L_{\text{ol}}}\right) \tag{2.1}$$

where L_{os} represents the short attenuation length, L_{ol} the long attenuation length, and the initial number of photons at $x = 0\,\text{cm}$ corresponds to $I_{\text{os}} + I_{\text{ol}}$.

For the PMT setup, attenuation length and total number of collected photons were determined using the same blue LED, driven by a Model PB-5 pulse generator (BNC) operating at 8.03 kHz, positive polarity, and 0.5 µs fall time. The LED was sequentially set at different positions along the fiber, and light at the fiber end was collected by the PMT. A WaveRunner 610Zi oscilloscope (10 GS/s) recorded both the LED trigger and PMT signal, ensuring that each acquisition corresponds to a controlled LED pulse.

Waveforms were digitized and integrated between −20 and 50 ns around the trigger. The resulting charge distributions were fitted with Gaussian functions representing electronic noise and single- and double-photoelectron events. A mean charge of $8.06 \pm 0.77\,\text{mV}\,\mu\text{s}$ per photoelectron was obtained at 1150 V. An alternative integration method produced consistent results, confirming calibration reliability.

For signal processing, a custom algorithm was implemented to reject unwanted events such as saturated or overlapping pulses. Baseline offset correction was applied by averaging pre- and post-pulse regions [10, 11]. The validated waveforms were integrated over a 0–40 µs window to compute the total collected charge. The charge distributions were fitted to Gaussian functions, and the number of photons was extracted from the centroid of the fits.

The attenuation length analysis employed the same double-exponential model, equation (2.1).

3 Results and discussion

3.1 Attenuation length — experimental determination

3.1.1 Saint-Gobain BCF-92

For the Saint-Gobain BCF-92 square wavelength-shifting fibers, light attenuation was quantified using a double-exponential model to assess comply with the physics case of WLS fibers. In order to understand the variation of the number of photons with distance and to compute the attenuation length of the fiber, each dataset corresponding to different fiber segments was fitted to a sum of two exponentials, figure 5.

2026 JINST 21 C01007

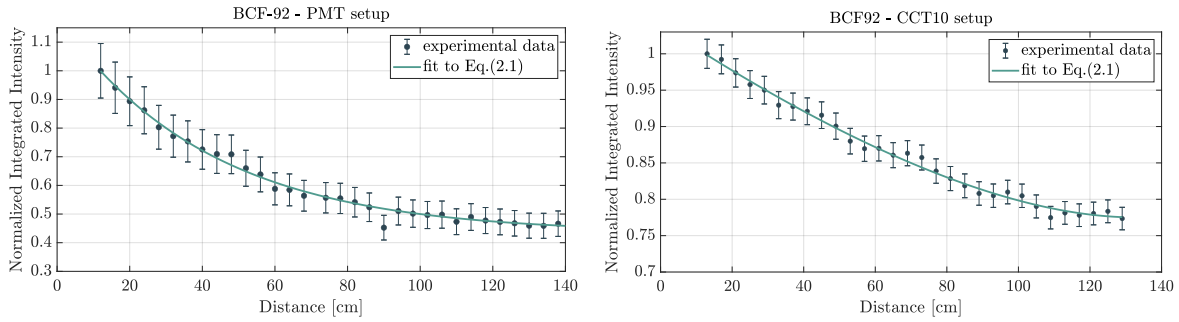

Figure 5. Double-exponential fit to the data taken with the PMT setup for the BCF-92 fiber (left) and double-exponential fit to the data taken with the spectrophotometer setup for the BCF-92 squared fiber (right).

The attenuation length of a WLS fiber can be decomposed into two components, namely a short attenuation length that dominates close to the readout point, and a long attenuation length that becomes significant at larger distances. The short attenuation length arises primarily from the absorption of shorter-wavelength light, e.g. $\lambda < 480\,\text{nm}$, blue and near-UV, within the fiber core or in light trapped inside the cladding. The long attenuation length, typically associated with longer-wavelength light, $\lambda \approx 500$–$550\,\text{nm}$, green, is affected by the reduction of losses from impurities, scattering, and structural defects. Optimizing this component requires careful control of fiber purity, uniformity, and manufacturing to minimize defects and bending losses [12, 13].

From the data acquired for the BCF-92 with the PMT setup, for the short component values were obtained ranging from 7.65 cm to 23.00 cm, with a mean value of $10.96 \pm 1.94\,\text{cm}$ (17.70%). The long component ranged from 169.25 cm to 333.33 cm, with a mean value of $285.06 \pm 30.35\,\text{cm}$ (10.65%).

The results demonstrate a high degree of consistency across multiple acquisitions and test conditions, indicating the robustness and reproducibility of the applied methodology. The long attenuation length (L_l) is well constrained, with relatively small associated uncertainties, reflecting the stability of the fit in this region. The short attenuation length (L_s) exhibits larger uncertainties, which can be attributed to the limited number of measurement points in the region close to the PMT,reducing the statistical accuracy of the fit and amplifying sensitivity to local fluctuations. Regarding the same fiber, for the spectrophotometer data the behavior is consistent, being both values for attenuation length higher ($L_l = 364.64 \pm 21.74\,\text{cm}$ and $L_s = 25.66 \pm 9.43\,\text{cm}$), as would be expected and is explained further on.

3.1.2 Kuraray Y11

Consistency in the measured behavior for the Y11 fiber was also verified across both methods, as illustrated in figure 6. The values for the long and short attenuation lengths were $L_l = 184.40 \pm 11.43\,\text{cm}$ and $L_s = 9.63 \pm 8.55\,\text{cm}$ for the PMT setup. For the spectrophotometer setup, the behavior was consistently higher, $L_l = 194.16 \pm 19.24\,\text{cm}$ and $L_s = 12.84 \pm 19.57\,\text{cm}$. Once more, the short attenuation length, L_s, exhibits larger uncertainties for the reason mentioned previously.

Overall, the analysis confirms that the dual-exponential model provides a reliable description of light attenuation in both studied fibers, with the long component yielding stable results across all runs. The observed variation in the short component remains within the expected range given the experimental constraints and does not compromise the validity of the measurements.

2026 JINST 21 C01007

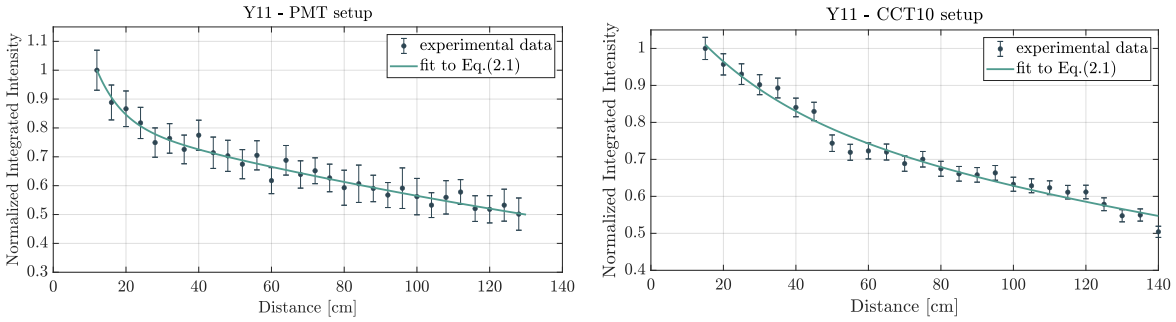

Figure 6. Attenuation length for Y11 with the PMT setup (left) and the spectrophotometer (right).

The spectrophotometer consistently renders a higher number of photons than the PMT method because it records the full emitted spectrum, while the PMT setup captures only the part of the light pulse within the PMT sensitivity wavelength region. As a result, although both methods show consistent attenuation behavior, the spectrophotometer method provides higher absolute number of photon.

3.2 Spectral analysis of the fiber emission

The spectral behavior of the fibers was studied to assess the response in terms of emission spectra with distance.

The emission spectra for both the BCF-92 and the Y11 fibers were collected at increasing distances from the LED to the input of the CCT10 spectrophotometer (figure 7).

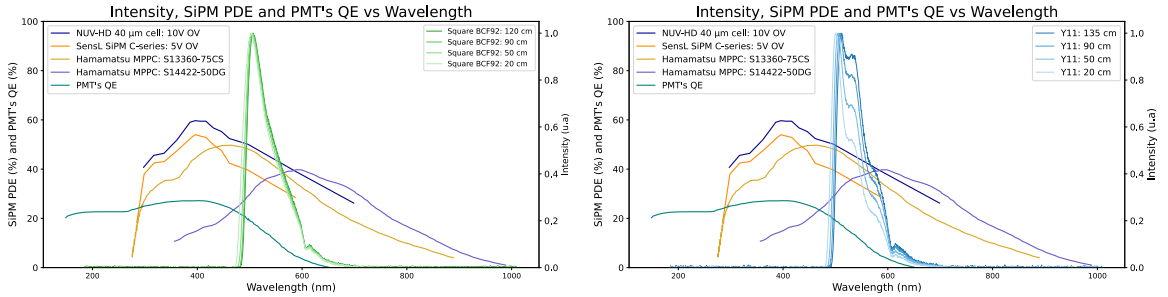

Figure 7. Emission spectra of the BCF-92 (left) and Y11 (right) fiber at increasing distances between the LED and the fiber input, collected with the CCT10 spectrophotometer. The quantum efficiency (QE) curve of the PMT and the photon detection efficiency (PDE) of different SiPM models are overlaid.

As expected, the overall intensity decreases with propagation due to attenuation. In addition, a progressive redshift of the emission peak is observed. This phenomenon is characteristic of WLS fibers and can be attributed to self-absorption and differential attenuation: shorter wavelength components within the emission band undergo stronger absorption and scattering, leading to their preferential suppression over longer path lengths. Consequently, the spectral centroid shifts towards longer wavelengths, where attenuation is less pronounced.

To evaluate the spectral compatibility to different photosensors, the measured fiber emission spectra were superimposed on the quantum efficiency (QE) curve of the PMT used in this work and the photon detection efficiency (PDE) curves of available SiPM models. These show a strong spectral overlap with the measured fiber emission, indicating high adequacy of those photosensors. The

2026 JINST 21 C01007

NUV-HD device under development at Fondazione Bruno Kessler (FBK) exhibits the highest PDE values in the relevant range. The Hamamatsu MPPC S13360-75C, a commercially available option, provides comparable PDE performance and presents itself as an adequate commercial candidate for integration in near-future fiber-based detection systems.

4 Conclusions

The dual component attenuation length of wavelength shifting (WLS) fibers was measured using two independent setups, namely a PMT readout and a spectrophotometer, and we modeled the attenuation as the sum of two exponentials.

To ensure the robustness of the results, approximately 70 independent runs were performed under the same experimental conditions but on different days, at different day-times and slightly different ambient temperatures. The four sides of the BCF-92 square fiber were also assessed independently. The reproducibility of the measurements demonstrates that random variations such as fluctuations in environmental conditions or photon counts were small, and overall consistency indicates that systematic effects were well controlled. This assures the reliability of the reported attenuation lengths and emission behaviors.

For the BCF-92 square fiber, the PMT method yields $L_s = 10.96 \pm 1.94$ cm and $L_l = 285.06 \pm 30.35$ cm, while the spectrophotometer method gives $L_s = 25.66 \pm 9.43$ cm and $L_l = 364.64 \pm 21.74$ cm. For the Y11 round fiber, the PMT method yields $L_s = 9.63 \pm 8.55$ cm and $L_l = 184.40 \pm 11.43$ cm, while the spectrophotometer method gives $L_s = 12.84 \pm 19.57$ cm and $L_l = 194.16 \pm 19.24$ cm. As expected, higher photon counts are recorded with the spectrophotometer relative to the PMT, which arises from the fact that the spectrophotometer integrates the entire emission band, while the PMT measures only the fraction within its sensitivity window; nevertheless, both methods return consistent attenuation behavior.

Results under different test conditions show that the applied methods for determining the attenuation length of WLS fibers are robust. The higher uncertainty in the short attenuation length compared to the long attenuation length is due to limited data in that region.

The consistency in the results obtained through the two independent setups/methods supports the validity of the two-component exponential model used to describe light attenuation along the fibers. While quantitative discrepancies, especially in the short component (L_s), are evident, the agreement in the overall behavior between both PMT and spectrophotometer setups is evident.

The spectrophotometer data confirms both the expected attenuation behavior and red-shifting in the fiber emission with increasing illumination distance to the collection position [14]. The comparison of the fiber emission curves with PDE curves from several commonly used photosensors shows the adequacy of the several sensor as the readout for the studied fibers,taking into account the commercial availability and their price.

Acknowledgments

This work is funded through FCT – Fundação para a Ciência e a Tecnologia, I.P., under Projects UIDP/04559/2020, UIDB/05559/2020, CERN/FIS-TEC/0038/2021, PTDC/FIS-NUC/3933/2021, CERN/FIS-INS/0026/2019, 2024.00269.CERN, UIDB/FIS/04559/2025, UIDP/FIS/04559/2025 (LIBPhys), funded through FCT by national funds and PRR, measure RE-C06-i06.m02. C.M.B. Monteiro acknowledges funding DOI: 10.54499/CEECIND/04434/2017/ CP1460/CT0027 from FCT.

2026 JINST 21 C01007

References

[1] NEXT collaboration, *Initial results of NEXT-DEMO, a large-scale prototype of the NEXT-100 experiment*, 2013 *JINST* **8** P04002 [arXiv:1211.4838].

[2] J.J. Csáthy et al., *Optical fiber read-out for liquid argon scintillation light*, arXiv:1606.04254.

[3] B. Cheymol, *Scintillator Detectors for the ESS High Energy Wire Scanner*, in the proceedings of the *57th ICFA Advanced Beam Dynamics Workshop on High-Intensity and High-Brightness Hadron Beams*, Malmö, Sweden (2016), MOPL018, p. 232–236 [DOI:10.18429/JACoW-HB2016-MOPL018].

[4] J.J. Gómez-Cadenas, *The NEXT experiment*, *Nucl. Part. Phys. Proc.* **273-275** (2016) 1732 [arXiv:1411.2433].

[5] Luxium Solutions, *Plastic Scintillating Fibers*, https://luxiumsolutions.com/sites/default/files/2021-11/Fiber-Product-Sheet.pdf (2024).

[6] K.L. Matthews, S.M. Leonard, C.E. Ordonez and W. Chang, *Comparison of wavelength-shifting fiber types and methods of ribbon assembly for the depth-encoding Anger detector*, in the proceedings of the *2001 IEEE Nuclear Science Symposium Conference Record (Cat. No.01CH37310)*, San Diego, CA, U.S.A. (2001), vol. 4, p. 1933–1936 [DOI:10.1109/nssmic.2001.1009202].

[7] Kuraray, *Wavelength Shifting Fibers*, http://kuraraypsf.jp/psf/ws.html (2025).

[8] ET Thorlabs, *CCT10, CCT11, CCT12 — CCT Spectrometer Series*, https://www.thorlabs.com/thorproduct.cfm?partnumber=CCT10 (2025).

[9] ET Enterprises, *C647 series data sheet*, http://et-enterprises.com/products/voltage-dividers (2024).

[10] C.A.O. Henriques et al., *Understanding the xenon primary scintillation yield for cutting-edge rare event experiments*, *JCAP* **06** (2024) 041 [arXiv:2309.14202].

[11] NEXT collaboration, *Neutral Bremsstrahlung Emission in Xenon Unveiled*, *Phys. Rev. X* **12** (2022) 021005 [arXiv:2202.02614].

[12] M.J. Moura-David, *Low Dose rate effects in scintillating and WLS fibers by ionizing radiation*, ATL-TILECAL-96-078 (1996).

[13] G. Keiser, *Optical Fiber Communications*, McGraw-Hill (2011) [ISBN: 978-0-07-338071-1].

[14] G. Knoll, *Scintillation Detector Principles*, in *Radiation Detection and Measurement*, Chapter 8, John Wiley & Sons, Inc. (2010), p. 223–275.

2026 JINST 21 C01007